

# mmCSM-AB: guiding rational antibody engineering through multiple point mutations

Yoochan Myung<sup>1,2</sup>, Douglas E.V. Pires<sup>1,2,3,\*</sup> and David B. Ascher<sup>1,2,4,\*</sup>

<sup>1</sup>Computational Biology and Clinical Informatics, Baker Institute, Melbourne, VIC 3004, Australia, <sup>2</sup>Structural Biology and Bioinformatics, Department of Biochemistry and Molecular Biology, Bio21 Institute, University of Melbourne, Parkville, VIC 3052, Australia, <sup>3</sup>School of Computing and Information Systems, University of Melbourne, Parkville, VIC 3052, Australia and <sup>4</sup>Department of Biochemistry, University of Cambridge, Cambridge CB2 1GA, UK

Received March 10, 2020; Revised April 18, 2020; Editorial Decision May 04, 2020; Accepted May 16, 2020

## ABSTRACT

While antibodies are becoming an increasingly important therapeutic class, especially in personalized medicine, their development and optimization has been largely through experimental exploration. While there have been many efforts to develop computational tools to guide rational antibody engineering, most approaches are of limited accuracy when applied to antibody design, and have largely been limited to analysing a single point mutation at a time. To overcome this gap, we have curated a dataset of 242 experimentally determined changes in binding affinity upon multiple point mutations in antibody-target complexes (89 increasing and 153 decreasing binding affinity). Here, we have shown that by using our graph-based signatures and atomic interaction information, we can accurately analyse the consequence of multi-point mutations on antigen binding affinity. Our approach outperformed other available tools across cross-validation and two independent blind tests, achieving Pearson's correlations of up to 0.95. We have implemented our new approach, mmCSM-AB, as a web-server that can help guide the process of affinity maturation in antibody design. mmCSM-AB is freely available at [http://biosig.unimelb.edu.au/mmcsm\\_ab/](http://biosig.unimelb.edu.au/mmcsm_ab/).

## INTRODUCTION

The ability of antibodies to selectively and specifically bind tightly to targets and sites considered undruggable, has seen them become a major focus of therapeutic and diagnostic applications in a wide range of diseases. This specificity can be so highly tuned that they can be used to even selectively recognize a unique missense mutation, leading to their successful application in personalized medicine (1,2). As anti-

body therapies become more common, new approaches to more quickly and cheaply optimize the binding affinity and specificity, known as antibody maturation, are increasingly necessary. While experimental approaches to explore antibody binding space have become more efficient, previously successful efforts have shown that at least two single-point mutations are generally needed, which do not necessarily lie only in the complementarity-determining regions (CDRs) (3). Exploring all possible permutations and combinations of mutations has therefore remained a bottleneck in the antibody development pipeline.

Increasing computational power has led to a number of different approaches to guide the rational engineering of antibody binding and specificity. Initial approaches used a range of techniques, including homology modelling (4), protein-protein docking (5–7), energy functions (8–10) and more recently machine learning-based approaches (11–13). While these have been successfully used in the development of a number of clinical antibodies, they have generally been limited to the analysis of single-point missense mutations, and have been shown to be only weakly correlated with experimentally measured changes.

We have previously shown that by using graph-based signatures to represent the wild-type residue environment we can accurately predict the effects of mutations on protein folding, stability (14–16), dynamics (17), function (18) and interactions (15,19–25). These have provided insights into genetic diseases (26–32), drug resistance (33–42), pharmacokinetics (43–46) and rational protein engineering (47). Extending this to look at antibody engineering, we developed mCSM-AB2 (25), which was able to more accurately predict the effects of single-point missense mutations on antibody binding affinity. However, at the time the representations used by mCSM-AB2 and the amount of data available, still limited its ability to screen for the additive or synergistic effects of combinations of mutations.

Here, we present a new approach, mmCSM-AB, as a web-server that enables rapid and deep evaluations of combinations of multiple mutations in antibody-antigen complexes

\*To whom correspondence should be addressed. Tel: +61 90354794; Email: david.ascher@unimelb.edu.au  
Correspondence may also be addressed to Douglas E. V. Pires. Email: douglas.pires@unimelb.edu.au

using graph-based signatures, sequence- and structure-based information. mmCSM-AB models were trained using single-point mutations and the effects of multiple mutations were assessed, outperforming other available tools across our validation set of experimentally measured changes with double to 14 mutations. mmCSM-AB will help to guide rational antibody engineering by analysing the effects of introducing multiple mutations on binding affinity.

## MATERIALS AND METHODS

### Datasets

Effects of single-point mutations on antibody-antigen binding affinity (in terms of  $K_D$ , given in molar) were collected for 62 complexes (Figure 1 and Supplementary Table S1) with known structures available at the Protein Data Bank. The quality of 3D structures was reviewed with the resolution and R-value (Figure S1) from the wwPDB X-ray structure validation report. Mutation information for wild-type and mutant was compiled from three different resources: AB-BIND (48), PROXiMATE (49) and SKEMPI2.0 (50).

Since the binding affinity of non-binders cannot be accurately measured, non-binders were excluded from our training dataset. This generated a final dataset of 905 single missense mutations, and 242 multiple missense mutations with experimentally measured changes in binding affinity. Binding affinities of wild-type and mutant structures were converted to binding energy ( $\Delta G$ , given in Kcal/mol) (Equation 1) and the effects of mutations expressed in terms of the change in binding energy ( $\Delta\Delta G$ , Equation 2).

$$\Delta G = RT \ln(K_D) \quad (1)$$

$$\Delta\Delta G = \Delta G_{\text{wild}} - \Delta G_{\text{mutant}} \quad (2)$$

**Training set.** The 905 single point mutation training set presented a skewed distribution, with an average  $\Delta\Delta G$  of  $-1$  kcal/mol (Supplementary Figure S2A). To avoid potential bias in our machine-learning models, we also included the hypothetical reverse mutations, as previously proposed (17,20,23,51). Only reverse mutations with a measured effect in affinity below 2 kcal/mol were considered, to avoid situations where the reverse mutation could potentially compromise binding, with a total of 735 reverse mutations being modelled. This resulted in a final training dataset of 1640 mutations with associated changes in binding affinity.

**Blind-test set.** To evaluate our approach on multiple point mutations, the curated set of 242 experimentally characterized multiple mutants was used (Supplementary Figure S2B). This included multi-point mutations ranging from 2 to 14 mutations (Supplementary Figure S2C). Based on the proportion of the number of multiple mutations, the 242 blind-test set was further divided into two subsets; 101 double and triple mutations and 242 all multiple missense mutations and assessed separately.

**Assessing additive and synergistic multiple point mutations.** To explore the role of additive and synergistic effects across

our dataset, we identified a set of 38 multiple point mutations, where each individual mutation had been experimentally characterized as a single-point missense mutation. Additive mutations were defined as when the sum of the individual mutations was within 1 kcal/mol of the multiple-point mutation. We identified 24 additive and 14 synergistic mutations.

**Non-binder dataset.** During data curation we identified 47 sets of multiple mutations, which when experimentally evaluated completely disrupted antigen binding. These were excluded from the training and test sets, but used for further evaluation of the mmCSM-AB models.

**Validation set.** We collected an additional 59 experimentally characterized multiple mutation complexes from a previous study benchmarking the performance of available methods in predicting effects of mutations on antibody-antigen affinity (52). This dataset was not present in our bind-test set, and was therefore used as a validation set to compare the performance of mmCSM-Ab with other methods.

All datasets used are available for download at [http://biosig.unimelb.edu.au/mmcs\\_m\\_ab/datasets/](http://biosig.unimelb.edu.au/mmcs_m_ab/datasets/).

### Mutation modelling and feature engineering

**Modelling mutant structures.** Modeller (v.9.21) (53) was used to build single point mutants as well as multiple mutants incrementally. Structures were submitted for energy minimization using FoldX (54).

**Graph-based signatures.** The mCSM graph-based signatures have been widely adopted to capture both the geometry and physicochemical properties of wild-type residue environment using the cutoff scanning matrix algorithm and the resulting pharmacophore changes upon mutation (15). mCSM signatures were the main feature class used to train the mmCSM-AB predictive method.

**Energetic terms.** FoldX was used to calculate interaction energies for both wild-type and modelled mutant structures.

**Interface properties.** To capture changes in interaction networks upon mutation, all non-covalent interactions in the wildtype and mutant structures were calculated using Arpeggio (55). The difference in the solvent accessible surface area between wild-type and mutant structures was calculated using DSSP (56). Additionally, the distance from the mutated sites to binding partner was also calculated.

**Evolutionary scores.** In order to capture residue conservation, we employed different evolutionary scoring measures. These include Position Specific Scoring Matrices (PSSMs) calculated from multiple sequence alignments using PSI-BLAST (57) on the non-redundant UniProtKB/SwissProt database and substitution scores from PAM30.

**Mutation distances.** To account for potential synergistic and compensatory effects of mutations, we also included information on the distances between the individual mutations.

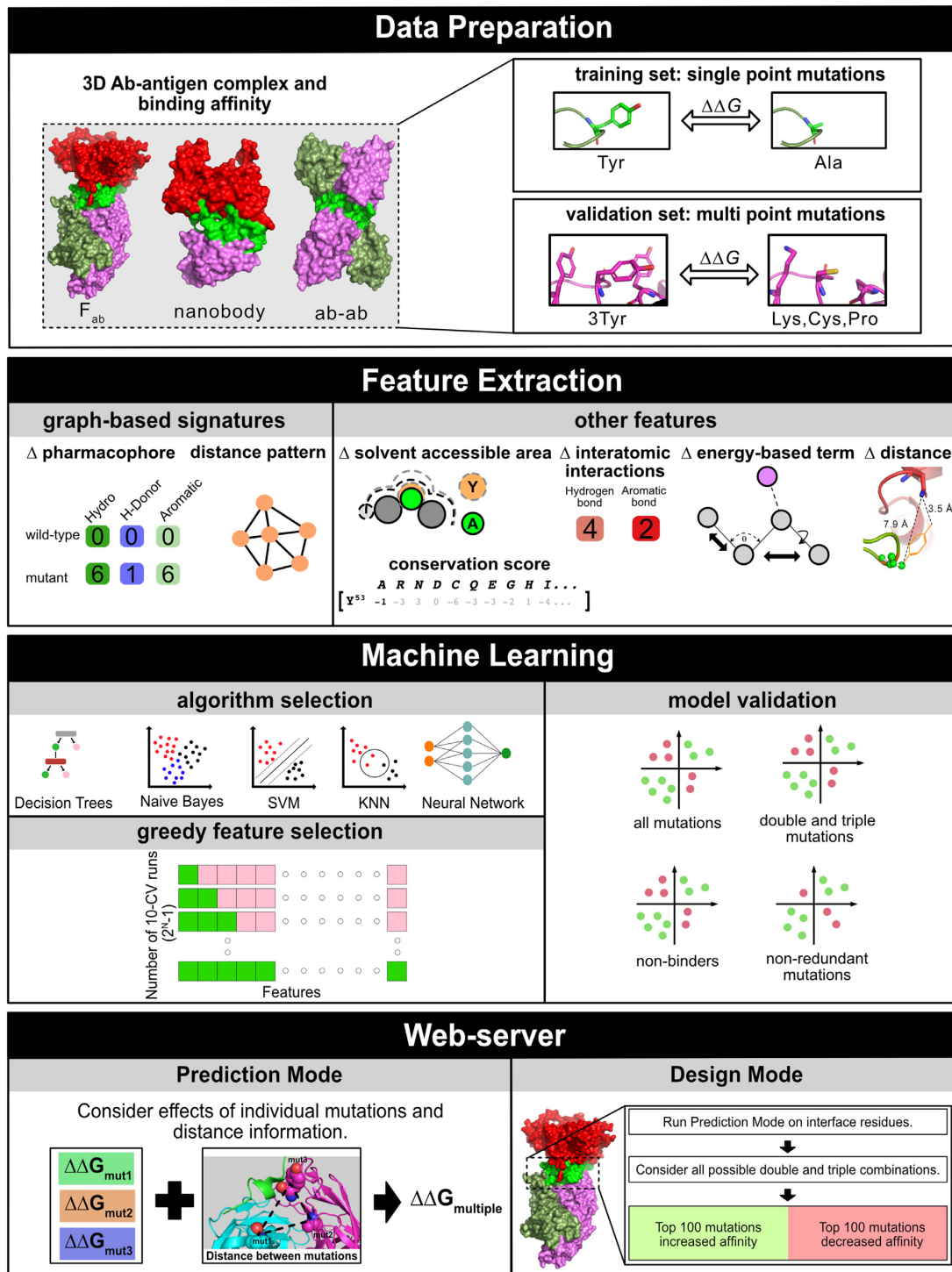


**Figure 1.** mmCSM-AB workflow. Method development can be divided into four steps. During data preparation, 905 single point mutation and 242 multi-point mutations across 62 complexes (50 Fab, 3 nanobody, 1 monobody, 1 Ab-Ab and 7 others described in Supplementary Table S1) were collected. During feature extraction, the curated 3D structures were used to calculate graph-based signatures as well as complementary structure- and sequence-based attributes. On the next step, these were provided as evidence to train and test supervised learning algorithms. Greedy feature selection was performed to optimize performance on multiple mutations and reduce dimensionality. On the last step, the best performing model was implemented into three prediction modes; the ‘Prediction mode’ for running user-specified mutations and the Antibody and Antigen Design modes, for systematically assessing permutation of multiple mutations on the antibody and antigen, respectively, at the binding interface.

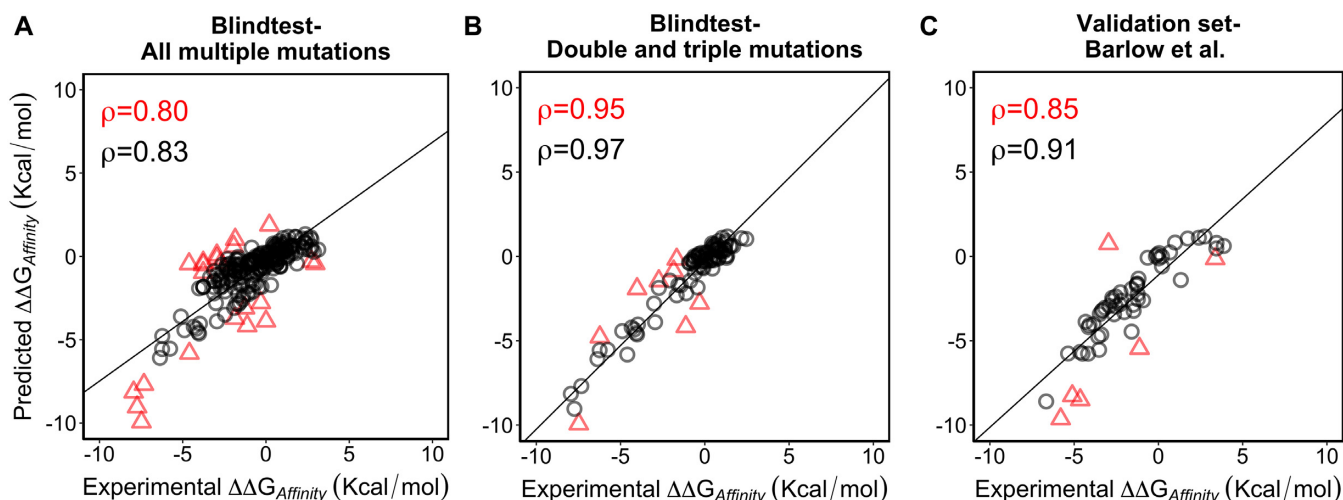


**Figure 2.** Performance of mmCSM-AB on multiple mutations. The figure depicts the performance of the final mmCSM-AB model on independent blind tests. The method achieved a Pearson's correlation of 0.80 (RMSE = 1.30) on all multiple missense mutations (242 in total) (A) and 0.95 (RMSE = 0.91) on double and triple mutation (101 in total) (B). Performance increases to 0.95 and 0.97, respectively, after 10% of outliers are removed. On an additional validation set comprised of 59 multiple mutations, mmCSM-AB achieved a correlation of 0.85 (RMSE = 1.66) (C), increasing to 0.91 across 90% of the data.

### Machine Learning

A range of supervised learning algorithms for regression currently available within the scikit-learn Python library were evaluated. These included Random Forest, Extra Trees, Gradient Boost, XGBoost, SVM and Gaussian Process. The best performing model was selected based on Pearson's correlation coefficient and Root Mean Squared Error (RMSE), evaluated under different cross-validation schemes (with 10 bootstrap repetitions), as well as blind tests. The best performing algorithm was ExtraTrees. In order to reduce dimensionality and improve performance, feature selection was carried out in an incremental stepwise greedy approach.

### WEB SERVER

mmCSM-AB was developed using Materialize 1.0.0 and Flask 1.0.2, and hosted on an Apache2 Linux server. This webserver is freely available at [http://biosig.unimelb.edu.au/mmcs\\_m\\_ab](http://biosig.unimelb.edu.au/mmcs_m_ab).

### Input

mmCSM-AB can analyse the effects of introducing multiple point mutations on antibody-antigen binding affinity. It can be used to either predict the effects of a known mutation via Prediction Mode, or systematic exploration of all potential multiple mutations at the interface to guide rational antibody engineering via Design mode (Supplementary Figure S3).

The server requires the user to provide (i) an antibody-antigen PDB structure either in a PDB file or PDB accession code; (ii) for Prediction Mode, provide a multiple mutation denoted by list of point mutations separated by semicolons, with mutations specified as the chain ID, wild-type residue one-letter code, residue number, and mutant residue one-letter code. Alternatively, users can upload a list of multiple mutations as a text file. Design mode automatically con-

siders all possible combinations of double- and triple-point mutations of residues on either the antibody or the antigen side of the interface.

### Output

The Prediction Mode result page consists of three sections. The mutation table shows predicted  $\Delta\Delta G$  (in kcal/mol) of a given multiple mutation and complementary details such as distance among single point mutations and distance to interface (Supplementary Figure S4). If the user provides more than one multiple mutation, the order of each result in the mutation table will be the same order as the given mutation list. Users can check wild-type atomic interactions of each of single point mutations via 3D molecular viewer, implemented using an NGL plugin (58). All results in the data table and 3D visualization can be downloaded as comma-separated file (CSV) and PyMOL session file (PSE), respectively.

The output of Design Mode shows the top 100 increasing/decreasing multi-point mutations at the binding interface of a given antibody-antigen complex (Supplementary Figure S5). Users need to select between stabilizing and destabilizing mutations in the mutation table to browse corresponding mutations. Similar to the Prediction Mode, each row of the mutation table provides information about antibody annotation, distance to interface and predicted  $\Delta\Delta G$ . By selecting the radio box in the first column, users can visualize the wild-type structure of each multi-point mutation in the 3D visualization section. All results of the mutation table are downloadable as a CSV file.

## VALIDATION

### Performance on cross-validation

In order to build a robust and reliable model for predicting the effects of mutations on antibody binding affinity,

**Table 1.** Performance comparison of available methods

Method	Blind-test											
	242 all mutations			101 double and triple mutations			104 unique all mutations			53 unique double and triple mutations		
	Pearson ( $\rho$ )	Spearman ( $\rho$ )	RMSE	Pearson ( $\rho$ )	Spearman ( $\rho$ )	RMSE	Pearson ( $\rho$ )	Spearman ( $\rho$ )	RMSE	Pearson ( $\rho$ )	Spearman ( $\rho$ )	RMSE
mmCSM_AB	0.80	0.78	1.30	0.95	0.89	0.91	0.77	0.72	1.15	0.92	0.84	0.66
mCSM_PPI	0.12***	0.12***	4.13	0.64***	0.36***	2.50	0.29***	0.23***	4.58	0.11***	0.01***	2.39
mCSM_PPI2	0.56***	0.45***	1.88	0.89**	0.76**	1.14	0.25***	0.23***	1.91	0.65***	0.58**	1.18
mCSM_AB	0.47***	0.39***	2.61	0.55***	0.32***	2.99	0.08***	0.01***	3.21	0.07***	0.31***	3.53
mCSM_AB2	0.66***	0.39***	2.84	0.88**	0.61***	3.40	0.45***	0.32***	2.29	0.62***	0.27***	1.91
DiscoveryStudio	0.63***	0.58***	1.83	0.76***	0.56***	1.79	0.48***	0.25***	1.50	0.67***	0.43***	1.27
DFIRE	0.52***	0.53***	1.93	0.70***	0.55***	2.14	0.36***	0.34***	1.52	0.48***	0.34***	1.36
bASA	0.47***	0.54***	71.08	0.68***	0.67***	57.76	0.32***	0.24***	43.20	0.57***	0.53**	50.22
dFoldX	0.45***	0.54***	2.06	0.54***	0.63***	2.20	0.44***	0.31***	1.73	0.68***	0.57**	1.29
SIPPER	0.41***	0.52***	3.59	0.43***	0.53***	3.45	0.36***	0.39***	2.49	0.44***	0.56**	2.26
ZRANK	0.37***	0.42***	7.23	0.40***	0.38***	7.95	0.34***	0.18***	8.78	0.46***	0.21***	10.11
dFIRE	0.33***	0.34***	2.15	0.70***	0.55***	2.14	0.36***	0.34***	1.52	0.48***	0.34***	1.36
PRODIGY	0.32***	0.37***	2.20	0.39***	0.46***	2.60	0.17***	0.16***	1.62	0.47***	0.37***	1.42
FIREDOCK	0.28***	0.28***	5.11	0.30***	0.24***	4.49	0.19***	0.05***	5.61	0.24***	0.09***	4.82
FIREDOCK_AB	0.26***	0.27***	5.52	0.26***	0.21***	4.70	0.19***	0.07***	5.90	0.19***	0.02***	5.17
ROSETTADOCK	0.19***	0.32***	2.32	0.19***	0.24***	2.69	0.22***	0.26***	1.78	0.34***	0.33***	1.47
ZRANK2	0.19***	0.62***	118.44	0.17***	0.67***	178.89	0.26***	0.37***	175.97	0.33***	0.55**	245.93
INSIDE	0.07***	0.01***	2.48	0.11***	0.02***	2.68	0.11***	0.03***	1.68	0.04***	0.15***	1.66
LISA	0.00***	0.04***	2.39	0.15***	0.16***	2.80	0.21***	0.26***	1.93	0.39***	0.49***	2.01

\*\* $P$ -value < 0.01, \*\*\* $P$ -value < 0.001; statistical significance of Pearson's correlation coefficient was evaluated by Fisher's  $r$ -to- $z$  transformation (two-tailed) and Spearman's rank-correlation coefficient was converted as described by Walker *et al.* (2003) into Pearson's correlation before we applied the transformation.

mmCSM-AB was trained using different stratified cross-validation approaches. We achieved Pearson's correlations up to 0.70 (RMSE = 1.03 kcal/mol) on 5-, 10- and 20-fold cross validation. We further validated the model, by performing a low redundancy leave-one-complex out validation, achieving a Pearson's correlation up to 0.64 (RMSE = 1.10 kcal/mol). Following feature selection using a greedy algorithm, we were left with a total of 83 features. Interestingly, the only features selected for the final model were the graph-based structural signatures, the evolutionary score and the Arpeggio calculated interactions.

### Performance on multi-point mutations

Our final mmCSM-AB model achieved a Pearson's correlation of 0.95 (RMSE = 0.91 kcal/mol, Figure 2) and 0.80 (RMSE = 1.30 kcal/mol, Figure 2) on the 101 double and triple mutations and the overall 242 multiple mutations, respectively (Table 1). Comparing the performance of mmCSM-AB to 18 alternative approaches, mmCSM significantly outperformed all methods across both mutation sets ( $P$ -value < 0.01, Fisher's  $r$ -to- $z$  transformation; Table 1). The inclusion of the hypothetical reverse mutations led to a significant improvement in performance. In particular, inclusion of hypothetical reverse mutations resulted in a final model with significantly improved ability to classify mutations as leading to increased binding affinity (Supplementary Table S2).

For comprehensive reviews of the performance in classifying favourable and unfavourable mutations across available methods, the predicted values from the comparative study (Table 1) were further classified as either increasing ( $\Delta\Delta G > 0.5$  Kcal/mol) or decreasing ( $\Delta\Delta G \leq -0.5$  kcal/mol) binding affinity. Using mmCSM-AB to classify mutations into these two categories, we achieved a Mathew's Correlation Coefficient (MCC) of 0.67 and  $F1$ -score of 0.89. Supplementary Figure S6 shows the corresponding ROC curves, with our predictor outperforming

other methods achieving an Area Under the ROC Curve (AUC) of 0.94.

To evaluate whether the performance relies on the training dataset, we filtered out 53 out of 101 double and triple mutations and 104 out of the overall 242 multiple mutations where none of the mutations was present in the training dataset. mmCSM-AB achieved a Pearson's correlation of 0.92 (RMSE = 0.66 kcal/mol, Table 1) and 0.77 (RMSE = 1.15 kcal/mol, Table 1) on the 53 unique double and triple mutations and the 104 unique mutations respectively, which demonstrates the robustness of our approach and its applicability to understand mutational effects upon diverse multi-point mutations.

### Performance on additive and synergistic multiple point mutations

From the 38 multiple mutations which have their individual  $\Delta\Delta G$ s from single-point mutation dataset, we identified 24 additive and 14 synergistic sets of multiple-point mutations. The mmCSM-AB model was evaluated across both sets, showing comparable performance regardless of whether the mutation effects were additive or synergistic. mmCSM-AB achieved a Pearson's correlation of 0.97 (RMSE = 0.84 kcal/mol) across the multiple point mutations identified as additive, and 0.94 (RMSE = 1.62 kcal/mol) across those identified as synergistic.

### Performance in ranking the effect of multiple point mutations

To guide rational antibody engineering, effective tools need to be able to identify the mutations leading to the greatest improvement in binding affinity. We therefore further assessed the ability of mmCSM-AB and available tools to ranking mutations in the order of most increasing and decreasing binding affinity. mmCSM-AB showed strong performance, achieving the Kendall's Tau and Spearman's rank-correlation coefficient up to 0.71 and 0.86 on the

242 multiple mutations, and outperforming all other approaches (Supplementary Table S3).

### Performance on non-binders

The mmCSM-AB model was further evaluated against the 47 data points where the introduction of multiple mutations led to complete disruption of antigen binding. mmCSM-AB correctly classified 46 out of 47 non-binders (Supplementary Table S4, 98% accuracy).

### Performance on external validation set

We further evaluated the performance of mmCSM-AB using the benchmark dataset from Barlow and colleagues (59). The 59 multiple mutations found in the antibody-antigen complexes did not appear in any other considered dataset and were used for performance comparison of available tools (Table 1). Considering all metrics in Supplementary Table S5, mmCSM-AB showed the second-best performance across 19 comparable methods, achieving a Pearson's correlation of 0.85 (RMSE = 1.66 kcal/mol).

## CONCLUSION

Here we introduce mmCSM-AB, a web server that uses our graph-based signatures to predict the effects of multiple-point missense mutations on antibody binding affinity. The method represents a significant advance upon our current predictive platform, outperforming previous methods, which have primarily been limited to single-point missense proteins. mmCSM-AB can assist antibody design efforts via a freely available, user-friendly and easy to use web server at <http://biosig.unimelb.edu.au/mmcsmb.ab>.

## SUPPLEMENTARY DATA

Supplementary Data are available at NAR Online.

## FUNDING

Y.M. was supported by the Melbourne Research Scholarship; D.B.A. and D.E.V.P. were funded by a Newton Fund RCUK-CONFAP Grant awarded by the Medical Research Council (MRC) and Fundação de Amparo à Pesquisa do Estado de Minas Gerais (FAPEMIG) [MR/M026302/1]; the Jack Brockhoff Foundation [JBF 4186, 2016]; Wellcome Trust [200814/Z/16/Z]; Investigator Grant from the National Health and Medical Research Council (NHMRC) of Australia [GNT1174405]; Victorian Government's OIS Program (in part). Funding for open access charge: MRC. *Conflict of interest statement.* None declared.

## REFERENCES

1. Yu, J., Kane, S., Wu, J., Benedettini, E., Li, D., Reeves, C., Innocenti, G., Wetzel, R., Crosby, K., Becker, A. *et al.* (2009) Mutation-specific antibodies for the detection of EGFR mutations in non-small-cell lung cancer. *Clin. Cancer Res.*, **15**, 3023–3028.
2. Watt, A.D., Crespi, G.A., Down, R.A., Ascher, D.B., Gunn, A., Perez, K.A., McLean, C.A., Villemagne, V.L., Parker, M.W., Barnham, K.J. *et al.* (2014) Do current therapeutic anti-Aβeta antibodies for Alzheimer's disease engage the target? *Acta Neuropathol.*, **127**, 803–810.
3. Sulea, T., Hussack, G., Ryan, S., Tanha, J. and Purisima, E.O. (2018) Application of Assisted Design of Antibody and Protein Therapeutics (ADAPT) improves efficacy of a *Clostridium difficile* toxin A single-domain antibody. *Sci. Rep.*, **8**, 2260.
4. Almagro, J.C., Teplyakov, A., Luo, J., Sweet, R.W., Kodangattil, S., Hernandez-Guzman, F. and Gilliland, G.L. (2014) Second antibody modeling assessment (AMA-II). *Proteins*, **82**, 1553–1562.
5. Sircar, A. and Gray, J.J. (2010) SnugDock: paratope structural optimization during antibody-antigen docking compensates for errors in antibody homology models. *PLoS Comput. Biol.*, **6**, e1000644.
6. Brenke, R., Hall, D.R., Chuang, G.Y., Comeau, S.R., Bohnuud, T., Beglov, D., Schueler-Furman, O., Vajda, S. and Kozakov, D. (2012) Application of asymmetric statistical potentials to antibody-protein docking. *Bioinformatics*, **28**, 2608–2614.
7. Cannon, D.A., Shan, L., Du, Q., Shirinian, L., Rickert, K.W., Rosenthal, K.L., Korade, M. 3rd, van Vlerken-Ysla, L.E., Buchanan, A., Vaughan, T.J. *et al.* (2019) Experimentally guided computational antibody affinity maturation with de novo docking, modelling and rational design. *PLoS Comput. Biol.*, **15**, e1006980.
8. Adolf-Bryfogle, J., Kalyuzhnyi, O., Kubitz, M., Weitzner, B.D., Hu, X., Adachi, Y., Schief, W.R. and Dunbrack, R.L. Jr (2018) RosettaAntibodyDesign (RABD): A general framework for computational antibody design. *PLoS Comput. Biol.*, **14**, e1006112.
9. Lippow, S.M., Witttrup, K.D. and Tidor, B. (2007) Computational design of antibody-affinity improvement beyond in vivo maturation. *Nat. Biotechnol.*, **25**, 1171–1176.
10. Pantazes, R.J. and Maranas, C.D. (2010) OptCDR: a general computational method for the design of antibody complementarity determining regions for targeted epitope binding. *Protein Eng. Des. Sel.*, **23**, 849–858.
11. Liberis, E., Velickovic, P., Sormanni, P., Vendruscolo, M. and Lio, P. (2018) Parapred: antibody paratope prediction using convolutional and recurrent neural networks. *Bioinformatics*, **34**, 2944–2950.
12. Olimpieri, P.P., Chailyan, A., Trantomano, A. and Marcotili, P. (2013) Prediction of site-specific interactions in antibody-antigen complexes: the proABC method and server. *Bioinformatics*, **29**, 2285–2291.
13. Daberdaku, S. and Ferrari, C. (2019) Antibody interface prediction with 3D Zernike descriptors and SVM. *Bioinformatics*, **35**, 1870–1876.
14. Pires, D.E., Ascher, D.B. and Blundell, T.L. (2014) DUET: a server for predicting effects of mutations on protein stability using an integrated computational approach. *Nucleic Acids Res.*, **42**, W314–W319.
15. Pires, D.E., Ascher, D.B. and Blundell, T.L. (2014) mCSM: predicting the effects of mutations in proteins using graph-based signatures. *Bioinformatics*, **30**, 335–342.
16. Pandurangan, A.P., Ochoa-Montano, B., Ascher, D.B. and Blundell, T.L. (2017) SDM: a server for predicting effects of mutations on protein stability. *Nucleic Acids Res.*, **45**, W229–W235.
17. Rodrigues, C.H., Pires, D.E. and Ascher, D.B. (2018) DynaMut: predicting the impact of mutations on protein conformation, flexibility and stability. *Nucleic Acids Res.*, **46**, W350–W355.
18. Rodrigues, C.H., Ascher, D.B. and Pires, D.E. (2018) Kinact: a computational approach for predicting activating missense mutations in protein kinases. *Nucleic Acids Res.*, **46**, W127–W132.
19. Pires, D.E., Blundell, T.L. and Ascher, D.B. (2015) Platinum: a database of experimentally measured effects of mutations on structurally defined protein-ligand complexes. *Nucleic Acids Res.*, **43**, D387–D391.
20. Pires, D.E. and Ascher, D.B. (2016) mCSM-AB: a web server for predicting antibody-antigen affinity changes upon mutation with graph-based signatures. *Nucleic Acids Res.*, **44**, W469–W473.
21. Pires, D.E. and Ascher, D.B. (2016) CSM-lig: a web server for assessing and comparing protein-small molecule affinities. *Nucleic Acids Res.*, **44**, W557–W561.
22. Pires, D.E., Blundell, T.L. and Ascher, D.B. (2016) mCSM-lig: quantifying the effects of mutations on protein-small molecule affinity in genetic disease and emergence of drug resistance. *Sci. Rep.*, **6**, 29575.
23. Pires, D.E.V. and Ascher, D.B. (2017) mCSM-NA: predicting the effects of mutations on protein-nucleic acids interactions. *Nucleic Acids Res.*, **45**, W241–W246.
24. Rodrigues, C.H.M., Myung, Y., Pires, D.E.V. and Ascher, D.B. (2019) mCSM-PP12: predicting the effects of mutations on protein-protein interactions. *Nucleic Acids Res.*, **47**, W338–W344.

25. Myung, Y., Rodrigues, C.H.M., Ascher, D.B. and Pires, D.E.V. (2020) mCSM-AB2: guiding rational antibody design using graph-based signatures. *Bioinformatics*, **36**, 1453–1459.
26. Jafri, M., Wake, N.C., Ascher, D.B., Pires, D.E., Gentle, D., Morris, M.R., Rattenberry, E., Simpson, M.A., Trembath, R.C., Weber, A. *et al.* (2015) Germline mutations in the CDKN2B tumor suppressor gene predispose to renal cell carcinoma. *Cancer Discov.*, **5**, 723–729.
27. Usher, J.L., Ascher, D.B., Pires, D.E., Milan, A.M., Blundell, T.L. and Ranganath, L.R. (2015) Analysis of HGD gene mutations in patients with alkaptonuria from the United Kingdom: Identification of novel mutations. *JIMD Rep.*, **24**, 3–11.
28. Nemethova, M., Radvansky, J., Kadasi, L., Ascher, D.B., Pires, D.E., Blundell, T.L., Porfiro, B., Mannoni, A., Santucci, A., Milucci, L. *et al.* (2016) Twelve novel HGD gene variants identified in 99 alkaptonuria patients: focus on ‘black bone disease’ in Italy. *Eur. J. Hum. Genet.*, **24**, 66–72.
29. Soardi, F.C., Machado-Silva, A., Linhares, N.D., Zheng, G., Qu, Q., Pena, H.B., Martins, T.M.M., Vieira, H.G.S., Pereira, N.B., Melo-Minardi, R.C. *et al.* (2017) Familial STAG2 germline mutation defines a new human cohesinopathy. *NPJ Genom Med.*, **2**, 7.
30. Trezza, A., Bernini, A., Langella, A., Ascher, D.B., Pires, D.E.V., Sodi, A., Passerini, I., Pelo, E., Rizzo, S., Nicolai, N. *et al.* (2017) A computational approach from gene to structure analysis of the human ABCA4 transporter involved in genetic retinal diseases. *Invest. Ophthalmol. Vis. Sci.*, **58**, 5320–5328.
31. Hnizda, P., Fabry, M., Moriyama, T., Pachel, P., Kugler, M., Brinsa, V., Ascher, D.B., Carroll, W.L., Novak, P., Zaliouva, M. *et al.* (2018) Relapsed acute lymphoblastic leukemia-specific mutations in NT5C2 cluster into hotspots driving intersubunit stimulation. *Leukemia*, **32**, 1393–1403.
32. Ascher, D.B., Spiga, O., Sekelska, M., Pires, D.E.V., Bernini, A., Tiezzi, M., Kralovicova, J., Borovska, I., Soltysova, A., Olsson, B. *et al.* (2019) Homogentisate 1,2-dioxygenase (HGD) gene variants, their analysis and genotype-phenotype correlations in the largest cohort of patients with AKU. *Eur. J. Hum. Genet.*, **27**, 888–902.
33. Ascher, D.B., Wielens, J., Nero, T.L., Doughty, L., Morton, C.J. and Parker, M.W. (2014) Potent heparinase C inhibitors bind directly to NS5A and reduce its affinity for RNA. *Sci. Rep.*, **4**, 4765.
34. Phelan, J., Coll, F., McNeerney, R., Ascher, D.B., Pires, D.E., Furnham, N., Coeck, N., Hill-Cawthorne, G.A., Nair, M.B., Mallard, K. *et al.* (2016) Mycobacterium tuberculosis whole genome sequencing and protein structure modelling provides insights into anti-tuberculosis drug resistance. *BMC Med.*, **14**, 31.
35. Hawkey, J., Ascher, D.B., Judd, L.M., Wick, R.R., Kostoulias, X., Cleland, H., Spelman, D.W., Padiglione, A., Peleg, A.Y. and Holt, K.E. (2018) Evolution of carbapenem resistance in *Acinetobacter baumannii* during a prolonged infection. *Microb Genom.*, **4**, e000165
36. Holt, K.E., McAdam, P., Thai, P.V.K., Thuong, N.T.T., Ha, D.T.M., Lan, N.N., Lan, N.H., Nhu, N.T.Q., Hai, H.T., Ha, V.T.N. *et al.* (2018) Frequent transmission of the Mycobacterium tuberculosis Beijing lineage and positive selection for the EsxW Beijing variant in Vietnam. *Nat. Genet.*, **50**, 849–856.
37. Karmakar, M., Globan, M., Fyfe, J.A.M., Stinear, T.P., Johnson, P.D.R., Holmes, N.E., Denholm, J.T. and Ascher, D.B. (2018) Analysis of a novel pncA mutation for susceptibility to pyrazinamide therapy. *Am. J. Respir. Crit. Care Med.*, **198**, 541–544.
38. Portelli, S., Phelan, J.E., Ascher, D.B., Clark, T.G. and Furnham, N. (2018) Understanding molecular consequences of putative drug resistant mutations in Mycobacterium tuberculosis. *Sci. Rep.*, **8**, 15356.
39. Vedithi, S.C., Malhotra, S., Das, M., Daniel, S., Kishore, N., George, A., Arumugam, S., Rajan, L., Ebenezer, M., Ascher, D.B. *et al.* (2018) Structural Implications of Mutations Conferring Rifampin Resistance in Mycobacterium leprae. *Sci. Rep.*, **8**, 5016.
40. Karmakar, M., Rodrigues, C.H.M., Holt, K.E., Dunstan, S.J., Denholm, J. and Ascher, D.B. (2019) Empirical ways to identify novel Bedaquiline resistance mutations in *AtpE*. *PLoS One*, **14**, e0217169.
41. Karmakar, M., Rodrigues, C.H.M., Horan, K., Denholm, J.T. and Ascher, D.B. (2020) Structure guided prediction of Pyrazinamide resistance mutations in *pncA*. *Sci. Rep.*, **10**, 1875.
42. Vedithi, S.C., Rodrigues, C.H.M., Portelli, S., Skwark, M.J., Das, M., Ascher, D.B., Blundell, T.L. and Malhotra, S. (2020) Computational saturation mutagenesis to predict structural consequences of systematic mutations in the beta subunit of RNA polymerase in Mycobacterium leprae. *Comput. Struct. Biotechnol. J.*, **18**, 271–286.
43. Pires, D.E., Blundell, T.L. and Ascher, D.B. (2015) pkCSM: predicting small-molecule pharmacokinetic and toxicity properties using graph-based signatures. *J. Med. Chem.*, **58**, 4066–4072.
44. Kaminskas, L.M., Pires, D.E.V. and Ascher, D.B. (2019) dendPoint: a web resource for dendrimer pharmacokinetics investigation and prediction. *Sci. Rep.*, **9**, 15465.
45. Chan, L.J., Bulitta, J.B., Ascher, D.B., Haynes, J.M., McLeod, V.M., Porter, C.J., Williams, C.C. and Kaminskas, L.M. (2015) PEGylation does not significantly change the initial intravenous or subcutaneous pharmacokinetics or lymphatic exposure of trastuzumab in rats but increases plasma clearance after subcutaneous administration. *Mol. Pharm.*, **12**, 794–809.
46. Chan, L.J., Ascher, D.B., Yadav, R., Bulitta, J.B., Williams, C.C., Porter, C.J., Landersdorfer, C.B. and Kaminskas, L.M. (2016) Conjugation of 10 kDa linear PEG onto trastuzumab Fab’ is sufficient to significantly enhance lymphatic exposure while preserving in vitro biological activity. *Mol. Pharm.*, **13**, 1229–1241.
47. Coelho, M.B., Ascher, D.B., Gooding, C., Lang, E., Maude, H., Turner, D., Llorian, M., Pires, D.E., Attig, J. and Smith, C.W. (2016) Functional interactions between polypyrimidine tract binding protein and PRI peptide ligand containing proteins. *Biochem. Soc. Trans.*, **44**, 1058–1065.
48. Sirin, S., Apgar, J.R., Bennett, E.M. and Keating, A.E. (2016) AB-Bind: Antibody binding mutational database for computational affinity predictions. *Protein Sci.*, **25**, 393–409.
49. Jemimah, S., Yugandhar, K. and Michael Gromiha, M. (2017) PROXiMATE: a database of mutant protein-protein complex thermodynamics and kinetics. *Bioinformatics*, **33**, 2787–2788.
50. Jankauskaite, J., Jimenez-Garcia, B., Dapkunas, J., Fernandez-Recio, J. and Moal, I.H. (2019) SKEMPI 2.0: an updated benchmark of changes in protein-protein binding energy, kinetics and thermodynamics upon mutation. *Bioinformatics*, **35**, 462–469.
51. Thiltgen, G. and Goldstein, R.A. (2012) Assessing predictors of changes in protein stability upon mutation using self-consistency. *PLoS One*, **7**, e46084.
52. Barlow, K.A., S.O.C., Thompson, S., Suresh, P., Lucas, J.E., Heinonen, M. and Kortemme, T. (2018) Flex ddG: Rosetta Ensemble-Based estimation of changes in Protein-Protein binding affinity upon mutation. *J. Phys. Chem. B*, **122**, 5389–5399.
53. Webb, B. and Sali, A. (2016) Comparative protein structure modeling using MODELLER. *Curr. Protoc. Bioinformatics*, **54**, 5.6.1–5.6.37.
54. Schymkowitz, J., Borg, J., Stricher, F., Nys, R., Rousseau, F. and Serrano, L. (2005) The FoldX web server: an online force field. *Nucleic Acids Res.*, **33**, W382–W388.
55. Jubb, H.C., Higuero, A.P., Ochoa-Montano, B., Pitt, W.R., Ascher, D.B. and Blundell, T.L. (2017) Arpeggio: A web server for calculating and visualising interatomic interactions in protein structures. *J. Mol. Biol.*, **429**, 365–371.
56. Kabsch, W. and Sander, C. (1983) Dictionary of protein secondary structure: pattern recognition of hydrogen-bonded and geometrical features. *Biopolymers*, **22**, 2577–2637.
57. Altschul, S.F., Madden, T.L., Schaffer, A.A., Zhang, J., Zhang, Z., Miller, W. and Lipman, D.J. (1997) Gapped BLAST and PSI-BLAST: a new generation of protein database search programs. *Nucleic Acids Res.*, **25**, 3389–3402.
58. Rose, A.S., Bradley, A.R., Valasatava, Y., Duarte, J.M., Prlic, A. and Rose, P.W. (2018) NGL viewer: web-based molecular graphics for large complexes. *Bioinformatics*, **34**, 3755–3758.
59. Jemimah, S. and Gromiha, M.M. (2018) Exploring additivity effects of double mutations on the binding affinity of protein-protein complexes. *Proteins*, **86**, 536–547.